PNAS
www.pnas.org

Supplementary Information for:

Structural insights into FTO's catalytic mechanism for the demethylation of multiple RNA substrates

Xiao Zhang[a,1], Lian-Huan Wei[a,1], Yuxin Wang[b, 1], Yu Xiao[a,1], Jun Liu[a], Wei Zhang[a], Ning Yan[c], Gubu Amu[c], Xinjing Tang[c], Liang Zhang[b, 2], Guifang Jia[a,d,2]

[a]Synthetic and Functional Biomolecules Center, Beijing National Laboratory for Molecular Sciences, Key Laboratory of Bioorganic Chemistry and Molecular Engineering of Ministry of Education, College of Chemistry and Molecular Engineering, Peking University, Beijing 100871, China.
[b]Department of Pharmacology and Chemical Biology, Shanghai Jiao Tong University School of Medicine, Shanghai 200025, China.
[c]State Key Laboratory of Natural and Biomimetic Drugs, School of Pharmaceutical Sciences, Peking University, Beijing 100191, China.
[d]Beijing Advanced Innovation Center for Genomics, Peking University, Beijing 100871, China.
[1]X.Z., L.H.W., Y.W. and X.Y. contributed equally to this work.
[2]To whom correspondence may be addressed. Email: guifangjia@pku.edu.cn or liangzhang2014@sjtu.edu.cn.

This PDF file includes:

www.pnas.org/cgi/doi/10.1073/pnas.1820574116

Supplementary Text

We finally scaled the overall resolution to 3.3Å and optimized the data by performing ellipsoidal truncation and anisotropic scaling using the diffraction anisotropy server (1). The structure was subsequently determined by molecular replacement using the published *apo* FTO structure (PDBID: 3LFM) (2) as the searching model. Electron density based model building was performed using the computer graphics program Coot (3), and the final structures were visualized using PyMol (4). The data collection and structure refinement statistics are summarized in *SI Appendix*, Table S1.

Apart from the aforementioned hydrophilic interactions with the oligonucleotide binding motifs of FTO, the 5' and 3' ends of the 10-mer ssDNA have few interactions with FTO. A1 at the 5' end is disordered due to a lack of any significant interactions between FTO and oligonucleotide. Instead, C3, T4, and T6 stack with C3', T4', and T6' from another complex through π-π interactions, stabilizing the terminal of ssDNA strand (*SI Appendix*, Fig. S12*A* and *B*). The base of A7 at the 3' end flips 180°, and is stabilized in a small groove next to the catalytic pocket. The phosphate of A7 is locked by K88 of FTO via H-bonds (*SI Appendix*, Fig. S12*B-D*).

Supplementary Materials and Methods

Cloning, Expression, and Purification of Wild-type and Mutation FTO. The human *FTO* gene (GenBank Accession No. NP_001073901.1) was subcloned into pET28a vector to generate a His_6-tagged fusion protein. The plasmids with site-directed mutants were constructed by Mut Express II Fast Mutagenesis Kit V2 (C214-01, Vazyme) using appropriate mutant primers (Table S2). Double mutation FTO was constructed based onthe single mutation. Wild-type and mutation FTO were expressed and purified following the procedures as previously reported (13). All of the proteins were indicated by SDS–PAGE analysis.

Cell line and Antibodies. HEK 293T/17 cells (CRL-11268, ATCC) and HeLa cells (CCL-2, ATCC) were maintained in DMEM (10-013-CVR, Corning) with 10% FBS (10438-026, ThermoFisher Scientific) and 1% 100×Penicillin Streptomycin (30-002-CI, Corning).

The antibodies used for western blot analysis were as follows: FTO (ab124892, Abcam), β-actin (TA-09, Zsbio).

Knockdown of *FTO*. *FTO* siRNA with the target mRNA sequence 5'-AAAUAGCCGCUGCUUGUGAGA -3' was ordered from GenePharma. The scrambled siRNA (A06001, GenePharma) was used as a negative control. Knockdown of *FTO* was carried out using Lipofectamine RNAiMAX (13778150, ThermoFisher Scientific) following the manufacturer's protocols. 72 h post the transfection; western blot assays were conducted to confirm the efficiency of *FTO* knockdown.

mRNA Isolation. Total RNA was isolated from transfected cells with TRIzol reagent (15596018, ThermoFisher Scientific). mRNA was extracted using Dynabeads $Oligo(dT)_{25}$ (61002, ThermoFisher Scientific) following the manufacturer's protocols. mRNA concentration was measured by NanoDrop.

FTO Demethylation Activity Assays. The demethylation activity assays (three biological replicates) were performed as previously described (13, 15) with limited modifications. Briefly, reaction mixtures (50 μl) contained the following components: the indicated amount of m^6A/m^6A_m-modified RNA oligoes or mRNA, the indicated amount of FTO wild-type or mutant proteins, 0.2 U/μl RiboLock RNase inhibitor (EO0381, ThermoFisher Scientific), 283 μM of $(NH_4)_2Fe(SO_4)_2$ $6H_2O$, 300 μM of α-KG, 2 mM of L-ascorbic acid and 50 mM of HEPES (pH 7.0). Note that 3mT-ssDNA demethylation reactionwas performed in HEPES (pH 6.5) buffer without RNase inhibitor.All of the demethylation reactions were incubated at 37 ℃ for indicated times and quenched by the addition of 1 mM of EDTA followed by heating for 5 min at 95 ℃. The sequence of oligos were shown in *SI Appendix,*Table S2.

Synthesis of m^6A_m Standard Nucleoside andPhosphoramidite. The synthesis of m^6A_m free nucleoside and phosphoramidite was depicted by the following Scheme. Commercially available 2′-*O*-methyladenosine **1** (2.8 g, 10.00 mmol, 1 eq.) was treated with acetic anhydride in pyridine under N_2 protection for 12 hours at 55 ℃to protect 3′, 5′-hydroxyls to give intermediate **2**. Treatment of **2** with iodomethane in acetonitrile at room temperature overnight converted **2** to **3**. Without further purification, **3** was treated with 7 M NH_3 in methanolfor 48 hoursat room temperature. The solution was concentrated in vacuo and the residue was then purified by flash chromatography with MeOH/DCM (1:30) to afford the desired product N6-methyl-2'-O-methyladenosine (m^6A_m free nucleoside) **4** as a foamy solid (1.6 g, 5.30 mmol). Yield of 53.2% totally from three steps mentioned above was obtained. **^{1}H NMR (400 MHz, DMSO-*d*$_6$)** δ 8.38 (s, 1H), 8.24 (s, 1H), 7.83 (s, 1H), 6.01 (d, *J* = 5.6 Hz, 1H), 5.44 (t, *J* = 5.6 Hz, 1H), 5.27 (d, *J* = 4.8 Hz, 1H), 4.39-4.34 (m, 2H), 4.00 – 3.98 (m, 1H), 3.70-3.67 (m, 1H), 3.60-3.55 (m, 1H), 3.30 (s, 3H), 2.96 (s, 3H) (*SI Appendix*, Fig. S14*A*). **^{13}C NMR (101 MHz, DMSO-*d*$_6$)** δ 155.10, 152.58, 148.01, 139.45, 119.84, 86.50, 85.89, 82.52, 68.84, 61.52, 57.48, 27.00 (*SI Appendix*, Fig. S14*B*).

N^6-2'-*O*-dimethyladenosine (m^6A_m) nucleoside **4** (885.4 mg, 3.00 mmol, 1 eq.) was treated with 4,4'- DiMethoxytrityl chloride (DMTCl) in pyridine under N_2 protection for 12 hours at room temperature. The solution was poured into 100 mL 5% $NaHCO_3$ and the organic layerwas extracted with 100 mL dichloromethane (DCM). The organic phase was washed with 100 mL 5% $NaHCO_3$ once again, dried over anhydrous $Na_2SO_4$and evaporated under vacuum. The residue was then purified by flash chromatography with DCM/MeOH (40:1 – 30:1) to afford the product N6-methyl-5'-O-DMT-2'-O-methyladenosine**5** (841.0mg, 1.40 mmol, 46.9%) as a white solid. **5** (250.0mg, 0.40 mmol, 1 eq.) was treated with 2-cyanoethyl N,N,N',N'-tetraisopropyl phosphorodiamidite in dichloromethane (DCM) under N_2 protection for 2 hours at room temperature. The solution was concentrated in vacuo and the residue was then purified by flash chromatography with ethyl acetate/PE/TEA (40:20:1) to afford the product N6-methyl-5'-O-DMT-2'-O-methyladenosine-3'-(2-cyanoethyl-N,N-diisopropyl)phosphoramidite**6** (293.0 g, 0.35 mmol, 87.8%) as a white foamy solid. **^{1}H NMR (400 MHz, CDCl$_3$)** δ 8.35 (d, *J* = 6.5 Hz, 1H), 7.49 – 7.40 (m, 2H), 7.38 – 7.19 (m, 9H), 6.81 (dt, *J* = 5.1, 3.7 Hz, 4H), 6.11 (dd, *J* = 5.2, 2.9 Hz, 1H), 5.85 (s, 1H), 4.73 – 4.64 (m, 1H), 4.65 – 4.54 (m, 1H), 4.36 (dt, *J* = 11.9, 4.0 Hz, 1H), 4.27 – 4.10 (m, 1H), 3.99 – 3.85 (m, 1H), 3.80 (d, *J* = 3.4 Hz, 6H), 3.63 – 3.53 (m, 3H), 3.40 – 3.32 (m, 1H), 3.21 (s, 3H), 2.78 (td, *J* = 6.2, 2.0 Hz, 1H), 2.64 (dt, *J* = 24.0, 6.8 Hz, 2H), 2.40 (t, *J* = 6.5 Hz, 1H), 1.30 (dd, *J* = 6.7, 5.7 Hz, 8H), 1.08 (d, *J* = 6.8 Hz, 4H) (*SI Appendix*, Fig. S14*C*). **^{13}C NMR (101 MHz, CDCl$_3$)** δ 158.55, 155.48, 153.24,

144.51, 143.12, 138.71, 135.67, 130.20, 130.13, 128.25, 127.83, 126.91, 120.53, 113.13, 86.61, 83.56, 82.28, 81.95, 63.17, 58.13, 55.22, 46.19, 45.30, 43.15, 24.56, 23.00, 20.15 (*SI Appendix*, Fig. S14*D*).**^{31}P NMR (162 MHz, $CDCl_3$)** δ 150.97 (s), 150.24 (s) (*SI Appendix*, Fig. S14*E*).

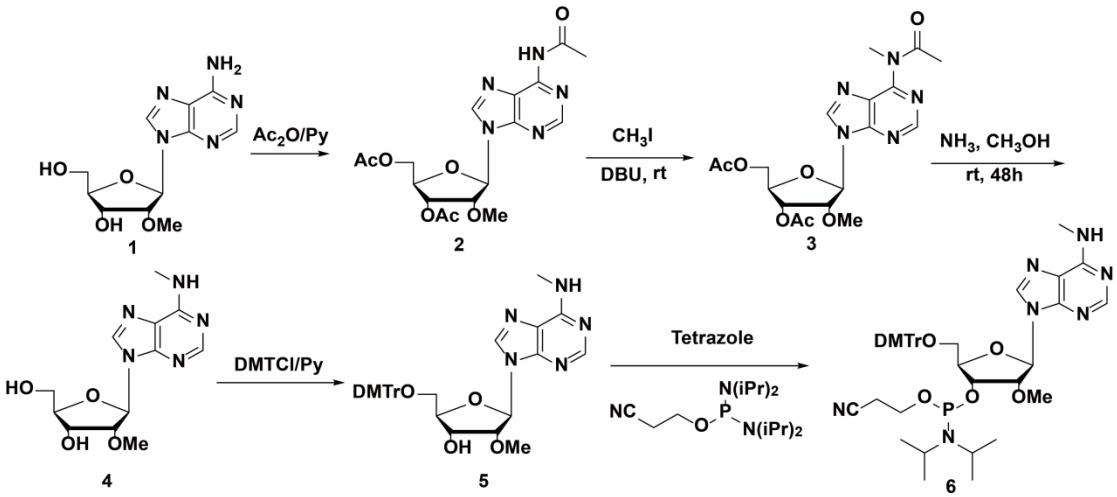

Scheme of synthesis of m^6A_m nucleoside and phosphoramidite from 2′-*O*-methyladenosine.

Measurement of mRNA Internal m^6A and Cap m^6A_m Levels Using UPLC-MS/MS. Ultra performance liquid chromatography tandem-mass spectrometry (UPLC-MS/MS) was used to measure mRNA internal m^6A and cap m^6A_m levels. Demethylated mRNA was purified by phenol chloroform extraction and ethanol precipitation. 200 ng purified mRNA was decapped with 20 units of RppH (M0356, NEB) in 1×Thermopol buffer (B9004S, NEB) for 3 h at 37 ℃. Decapped mRNA was subsequently digested to single nucleotides with 1 unit of Nuclease P1(145-07741, Wako) in 10 mM NH_4Ac for 2 h at 42°C. 5′ phosphates were removed with 1 unit of rSAP (M0371, NEB) in 100 mM MES (pH 6.5) for 3 h at 37 ℃.

The digested sample was filtered through a 0.22 μm syringe filter prior to injection into UPLC-MS/MS. The nucleosides were separated by UPLC (SHIMADZU) equipped with ZORBAX SB-Aq column (827975-914, Agilent), and detected with Triple Quad^{TM} 5500 (AB SCIEX) in positive ion multiple reaction-monitoring (MRM) mode. Quantitation of modifications was based on nucleoside-to-base ion mass transitions: m/z 268.0 to 136.0 for A, m/z 282.0 to 150.1 for m^6A, and m/z 296.0 to 150.0 for m^6A_m. The commercial A (PR 3005, Berry & Associates), m^6A (PR 3732, Berry & Associates) and synthesized m^6A_m nucleosides were used to generate standard curves, from which the concentrations of A, m^6A and m^6A_m in the samples were calculated. The level of m^6A orm^6A_m was then calculated as a percentage of total unmodified A.

Oligonucleotides Synthesis and Purification. DNA/RNA oligonucleotides (*SI Appendix*, Table S2) were synthesized on an Exptide 8909 DNA synthesizer using standard reagents. Oligonucleotides were subsequently deprotected and purified by standard methods recommended by Glen Research Corp. All purified oligonucleotides were verified by MALDI-TOF/TOF Mass Spectrometer 5800 (AB SCIEX).

Fluorescence Anisotropy Assay. 20 nM of Fluorescein-labeled 6mA-modified ssDNA (FAM-6mA-DNA, *SI Appendix* Table S2) was incubated with the increasing concentrations (10 to 10^4 nM) of wild-type and mutation FTO in 50 mM Tris-HCl buffer (pH 7.0) for 0.5 h at room temperature. Fluorescence anisotropy was measured at 25 ℃on a Synergy 4 Microplate Reader (BioTek) using the wavelengths of 480 nm for excitation and 535 nm for emission, respectively.

Measurement of 3mT, m^6A, and m^6A_m Levels in OligonucleotidesUsing HPLC. Oligonucleotides digested by nuclease P1 and alkaline phosphatase were analyzed on a HPLC system (Agilent 1260 Infinity) equipped with a Venusll MP C18 analysis column (5 μm, 150×4.6 mm, Bonna-Agela Technologies) and eluted with buffer A (50 mM NH_4Ac) and buffer B (50 mM NH_4Ac, 50% acetonitrile). Samples were analyzed at1 ml min^{-1} flow rate with the following buffer A/B gradient: 2 min 95%/5%, 20 min 80%/20%, 25 min 20%/80%, 28 min 95%/5%. The detection wavelength was set at 266 nm.

Crystallization. Crystals of the FTO-6mA complex were generated using the sitting drop vapor diffusion method. FTO Q86KQ306K (4.5 mg/mL) and 6mA-ssDNA (*SI Appendix*, Table S2) were incubated with the molecular ratio 1:1 in the mixture containing 3 mM of oxalylglycine (NOG) and 3 mM of Mn^{2+}. The mixture was incubated on ice for 30 min before setting up the crystallization. FTO-DNA complex was crystallized with reservoir solution [0.2M Sodium L-tartrate dibasic dehydrate (STDD, pH 7.0), and 20% (w/v) PEG 8000]. The crystals were obtained after 24 h at 16 ℃.

Data Collection and Structure Determination. The crystals were cryoprotected using 20% (v/v) glycerol and flash frozen in liquid nitrogen. The diffraction data of FTO-6mA complex was collected at BL19U (NCPSS) under wavelength at 0.9765 Å. The diffraction data was processed using HKL3000 software package. The significant anisotropy property of the diffraction during data collection (b and c direction to 3.0Å and 3.1Å, while a direction to 3.7Å) caused the overall resolution cut-off at 3.3 Å, and the data was further optimized by performing ellipsoidal truncation and anisotropic scaling on the diffraction anisotropy server (http://services.mbi.ucla.edu/anisoscale/). The structure was subsequently solved by using molecular replacement with the published FTO structure (pdb code: 3LFM) as the searching model. The electron density based model building was performed by using the computer graphics program Coot, and refined by using the program Phenix suit. The final structures were visualized by PyMol software. The crystallographic statistics were summarized in *SI Appendix*, Table S1.

Statistical Analysis. Student's unpaired t-test (two-tailed) was applied for statistical analysis using Graph- Pad Prism5.0 software.

Supplementary Figures

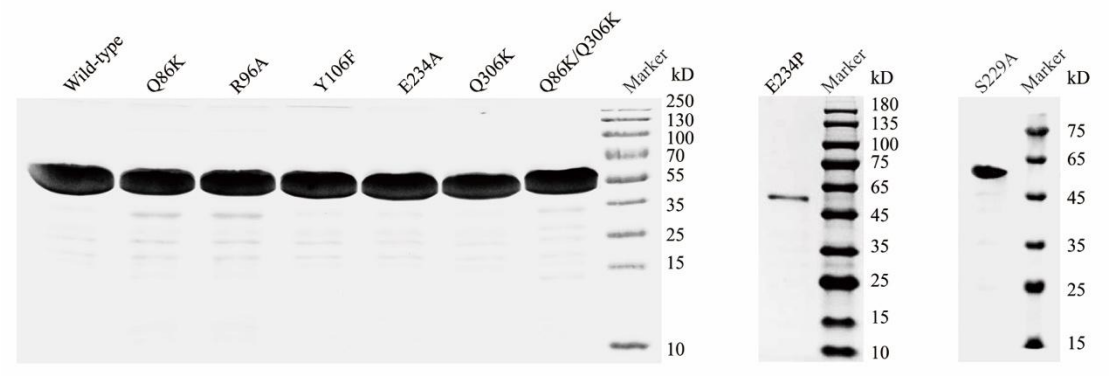

Fig. S1. SDS-PAGE analysis of purified FTO mutations.

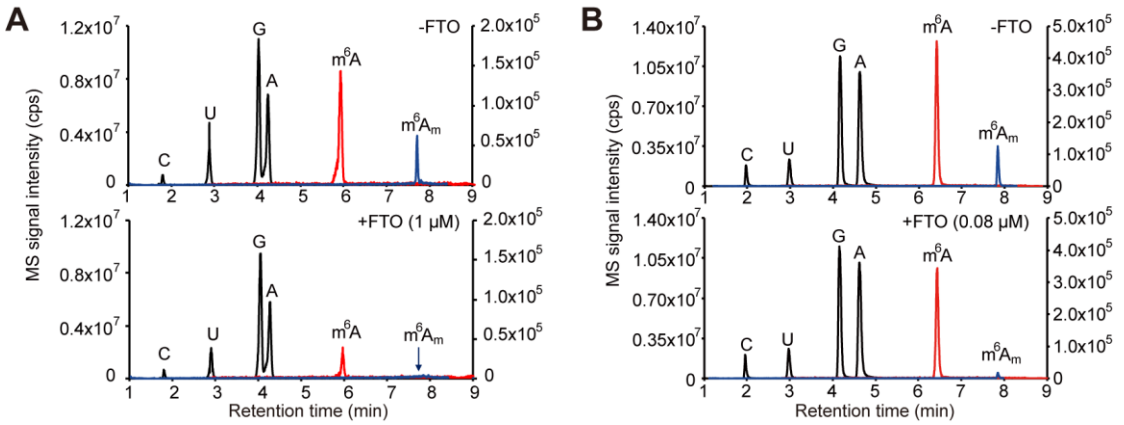

Fig. S2. Representative UPLC-MS/MS chromatograms of purified HeLa mRNA treated with FTO. The chromatograms of C, U, G and A are scaled to the left y axis, and the chromatograms of m^6A (red), m^6A_m (blue) are scaled to the right y axis. Signals according to m^6A and m^6A_m significantly decreased after treated with FTO.cps, counts per second.(**A**) 400 ng of purified HeLa mRNA was treated with 1 μM of FTO for 1 h at 37 °C (50 μl of reaction mixture). (**B**) 400 ng of purified HeLa mRNA was treated with 0.08 μM of FTO for 1 h at 37 °C (50 μl of reaction mixture).

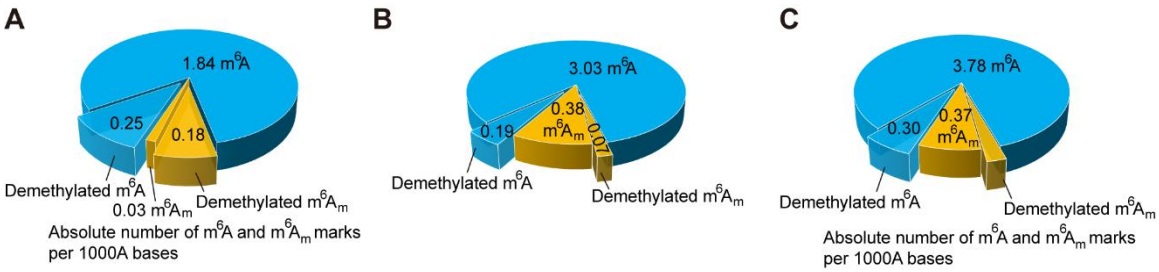

Fig. S3. The number of demethylated m^6A or m^6A_m per 1000 A calculated from Fig. 1B (**A**), Fig.1C (**B**), and Fig. 1D (**C**).

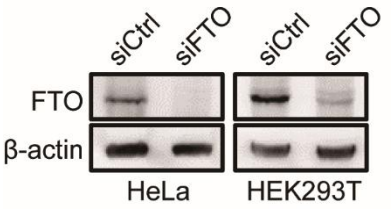

Fig. S4. The level of FTO protein in the *FTO* knockdown HeLa cells and HEK293T cells, whichwas indicated by western blot. β-actin was used as a loading control.

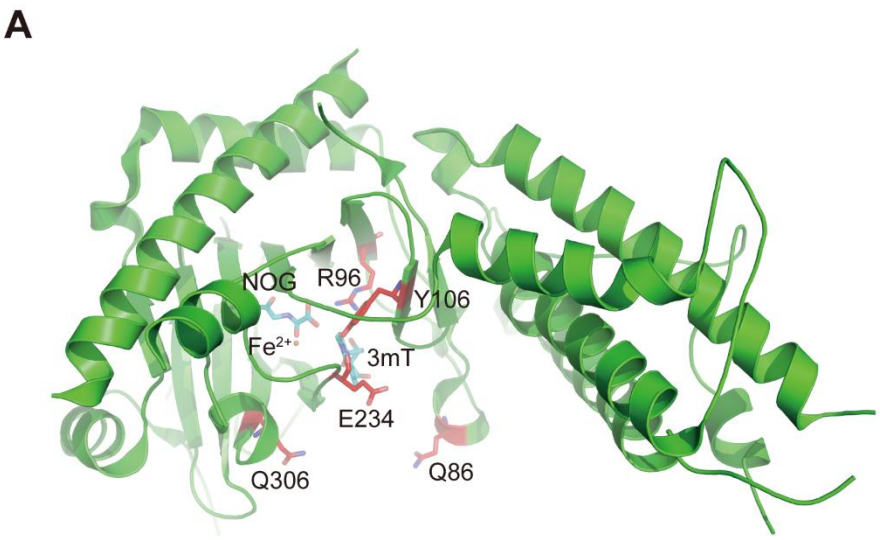

B

FTO	K_d (μM)
WT	3.69±0.62
R96A	7.45±0.48
Y106F	6.83±0.75
E234A	3.66±0.16
Q86K	2.53±0.43
Q306K	0.34±0.03
Q86K/Q306K	0.23±0.04

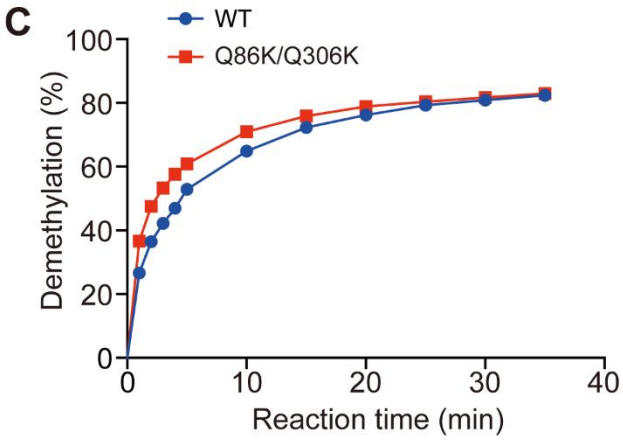

Fig. S5. Rational design of FTO mutation for crystallization of the complex of FTO bound 6mA-modified oligonucleotide. (A) Mutation sites of FTO selected for substrate binding evaluation. (**B**)The binding affinity of FTO mutations with Fluorescein-labeled 6mA-modified ssDNA (FAM-6mA-DNA) as a substrate. **(C)** The m^6A demthylation activity of 2 μM of FTO^{WT} and $FTO^{Q86K/Q306K}$ protein with Oligo2 (10 μM) for the indicated time at 37 ℃. Data indicate the mean ± s.e.m. (n=6, three biological replicates × two technical replicates).

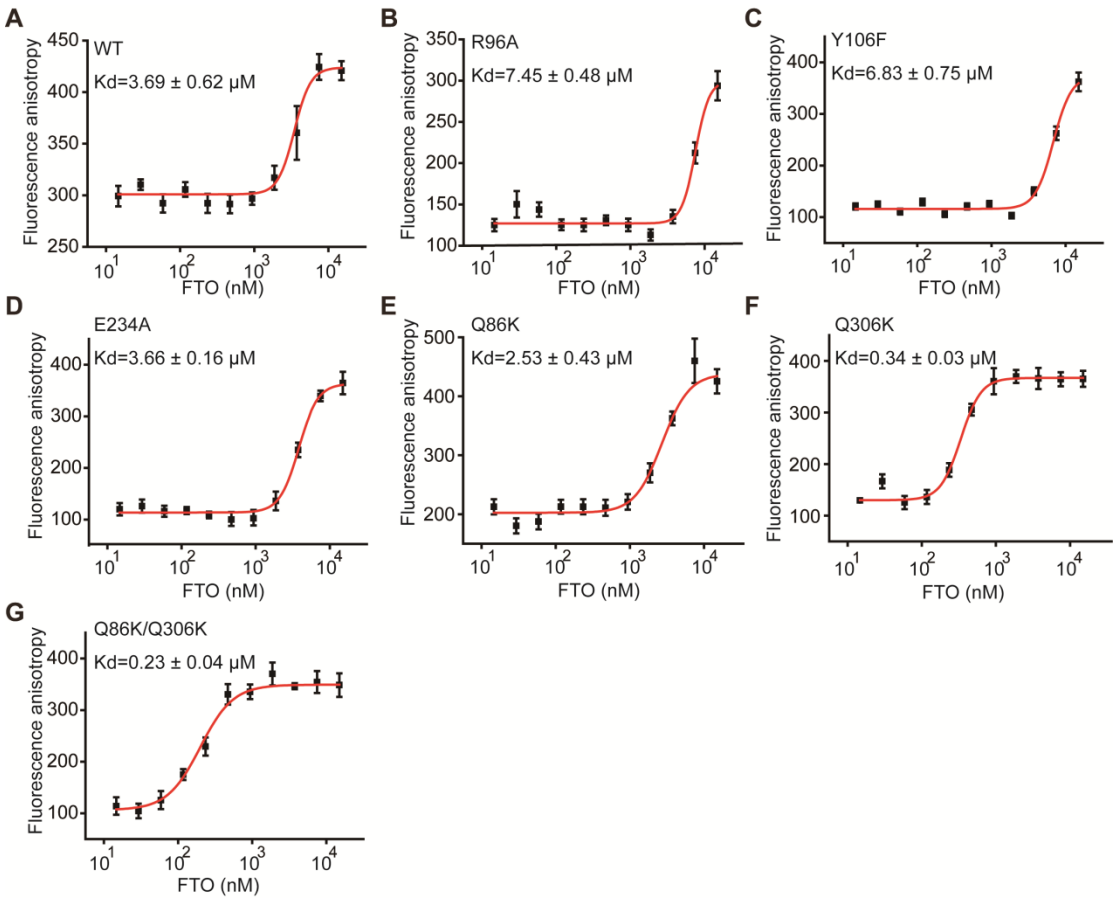

Fig. S6. The binding affinity of FTO mutations with 6mA-modified ssDNA. Fluorescein-labeled 6mA-modified ssDNA (20 nM) was incubated with increasing concentrations (10 to 10^4 nM) of FTO mutations for 0.5 h at room temperature, and the binding affinity was measured as change in anisotropy. FTO mutants Q86, Q306 and Q86/Q306 significantly increased the affinity with 6mA -modified ssDNA(~1.5 folds , ~10 folds, ~16 folds) while ~2-fold decrease for FTO mutants R96A, Y106F and no obvious change for FTO E234A. Error bars indicate mean ± s.e.m. (n=6, three biological replicates × two technical replicates).

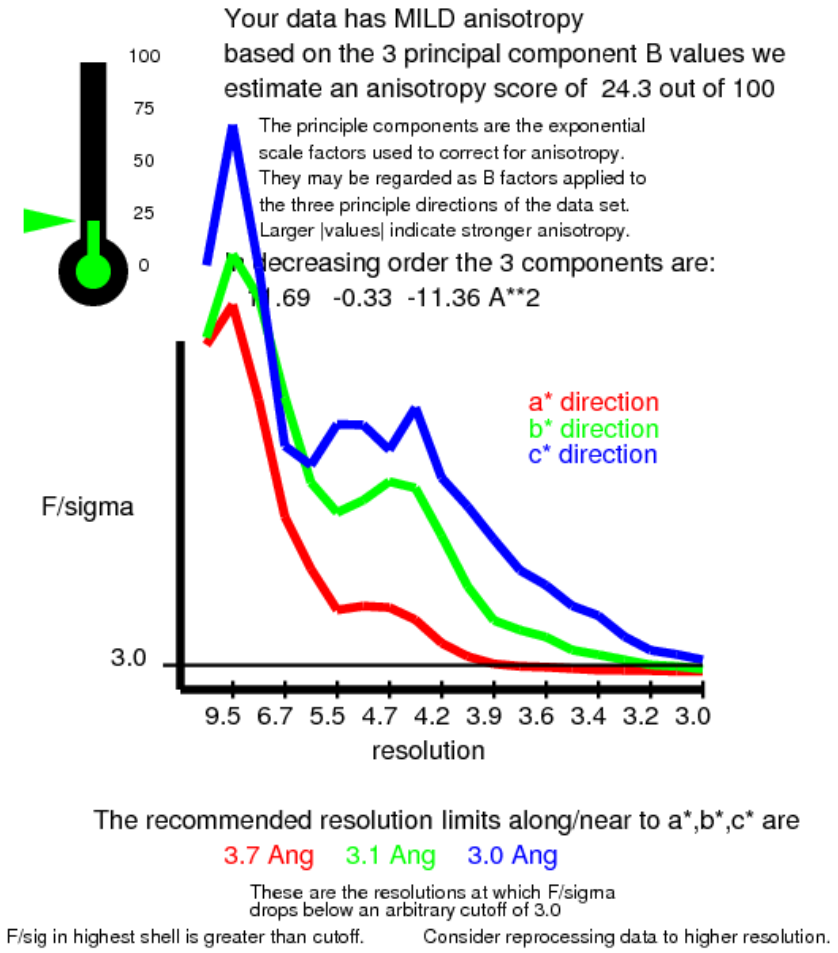

Fig. S7. Diffraction anisotropy analysis by the server. The results show that the FTO-6mA complex structure has mild anisotropy.

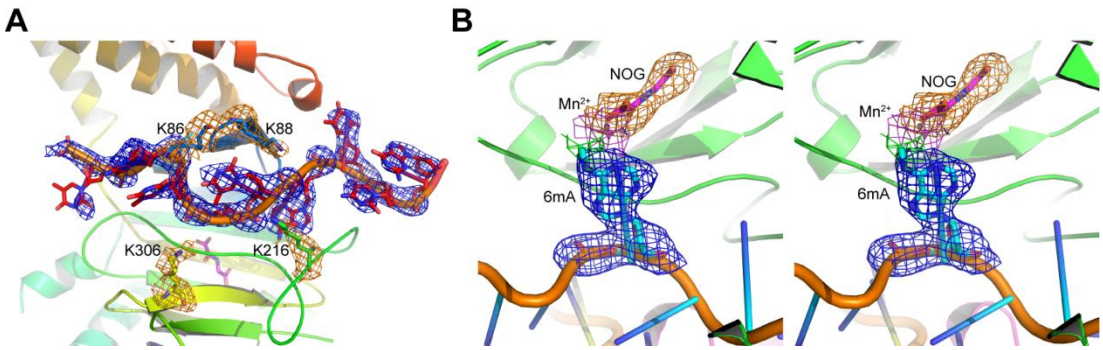

Fig. S8. Omit electron density map of 6mA-modified ssDNA and key residues of FTO at 3.0 σ. (A) The omit map of 6mA modified ssDNA and key residues of FTO are shown in blue and brown. (B) The omit map of 6mA and NOG are shown in blue and brown. The electron density map of N^6-methyl group of 6mA is colored in green at 3.0 σ. The anomalous density map of Mn^{2+} is colored in purple at 3.0 σ.

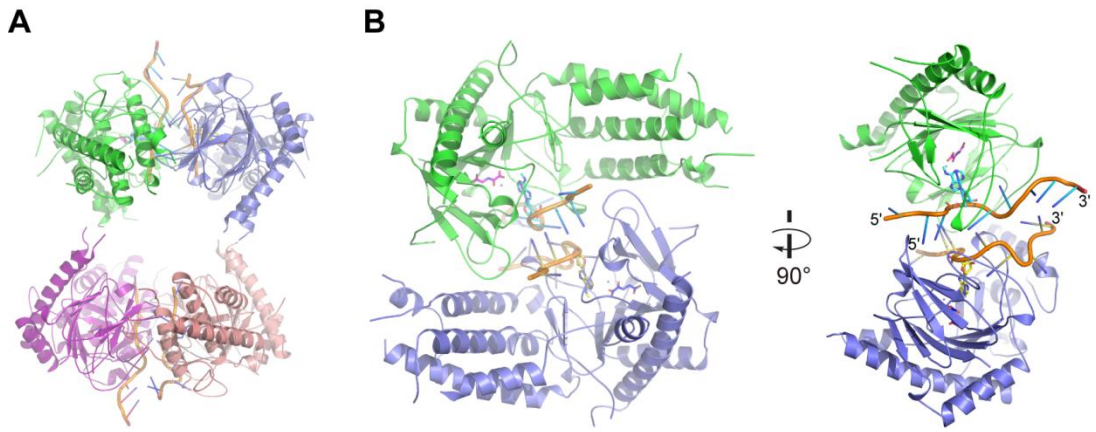

Fig. S9. Overall structure of FTO bound to 6mA-modified ssDNA. **(A)** Four FTO and ssDNA molecules are colored in green, purple, wheat, slate, cyan, yellow, red, and blue. **(B)** Two NOG molecules are colored in magenta and purple respectively.

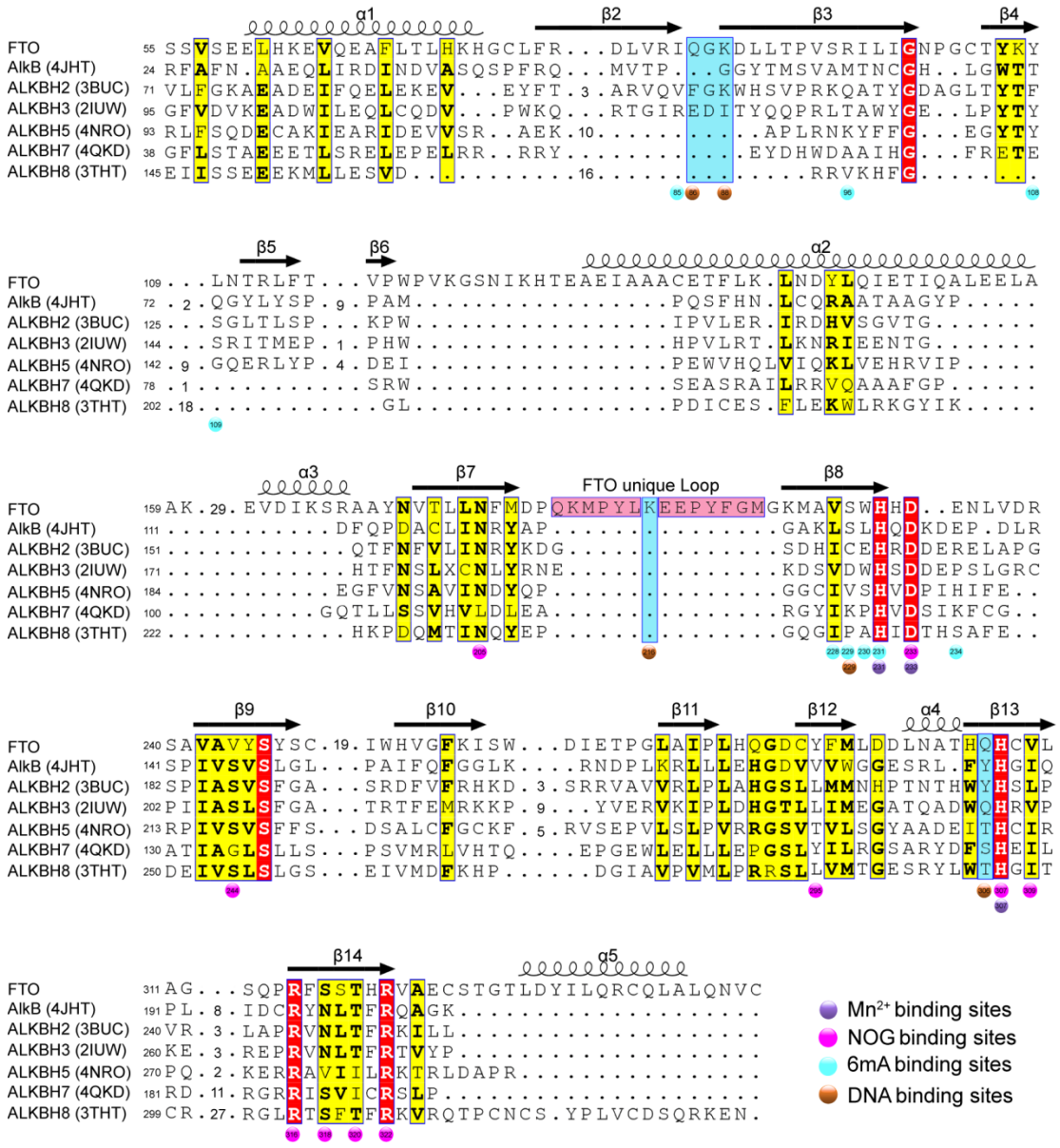

Fig. S10. Structural sequence alignment through the AlkB family. Residues involved in interactions with 6mA, NOG, Mn^{2+} and DNA are labeled with cyan, magenta, pruple and brown disk. The secondary structure of FTO are shown and labeled. The unique loop of FTO is colored in pink.

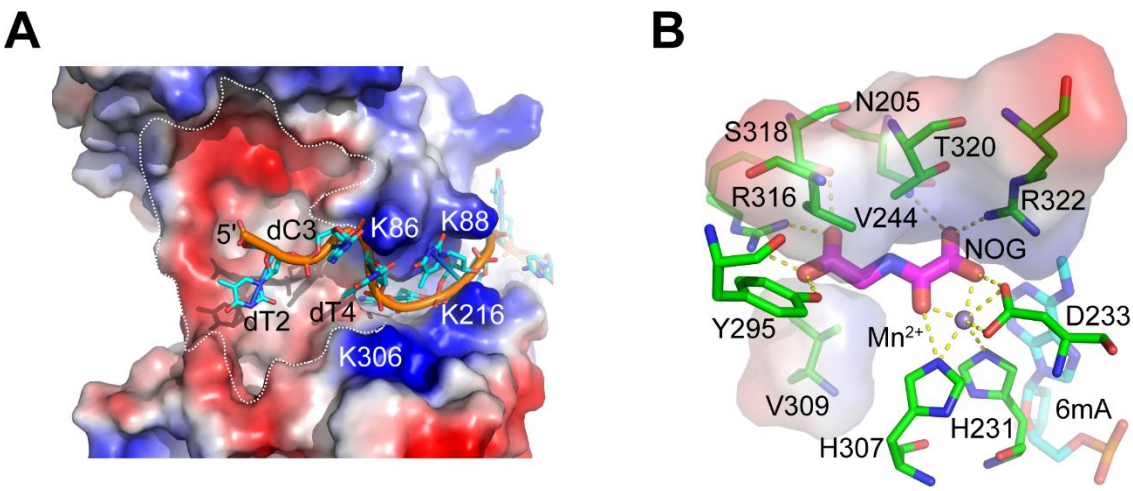

Fig. S11. Crystal structure of FTO bound to 6mA-modified ssDNA. (**A**) The electrostatic surface of the large space next to Pincer 2 for potential accommodation of RNA with tertiary structures like stem loops. **(B)** Detailed interactions in the catalytic pocket of FTO to accommodate NOG and Mn^{2+}. FTO, 6mA-modified ssDNA, 6mA nucleotide, and NOG are colored in green, cyan, and magenta, respectively. Residues and nucleotides involved in the interactions are labeled and shown as sticks. The Mn^{2+} ion is shown as a purple sphere. The H-bond network is shown as yellow dashes, and distances are labeled.

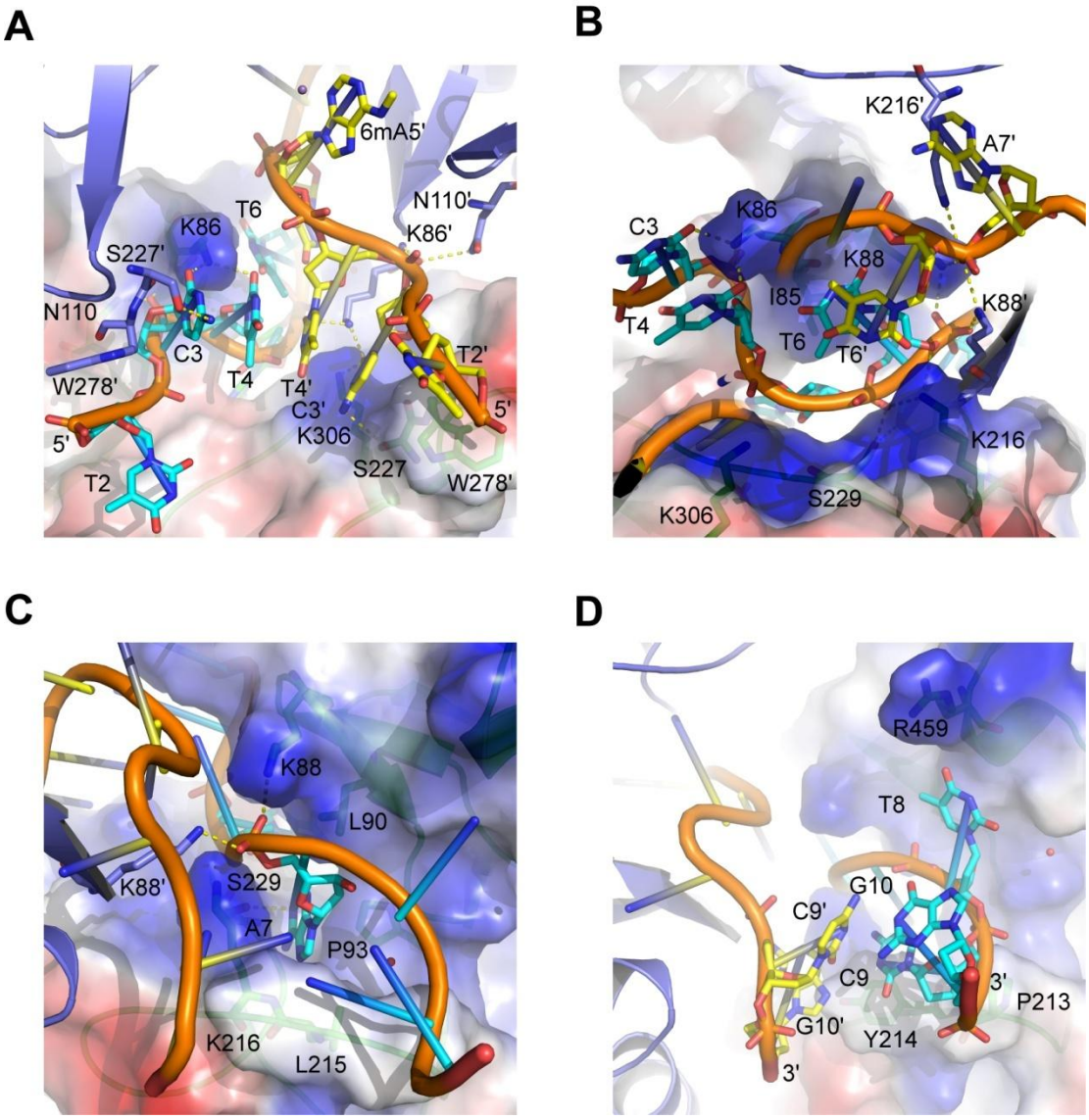

Fig. S12. The detailed interactions of FTO with ssDNA. Two FTO molecules are colored in green and slate. Two ssDNA are colored in cyan and yellow. **(A)** Interactions in 5' end of ssDNA. **(B)** Interactions in middle of ssDNA. **(C)** Interactions near the active site of ssDNA. **(D)** Interactions in 3' end of ssDNA.

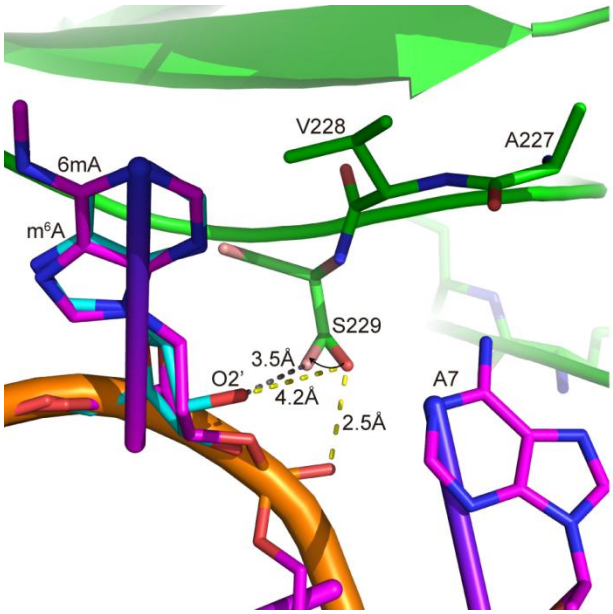

Fig. S13. Superposition of m^6A nucleoside (cyan) with 6mA (magenta). Residues and nucleotides near the O2' positon of 6mA ribose ring are shown and labeled. The dashes indicate the distance between the sidechain of Ser229 in the structure (yellow) or after a potential sidechain rotation (gray) and the hydroxyl group on the O2' positon of m^6A.

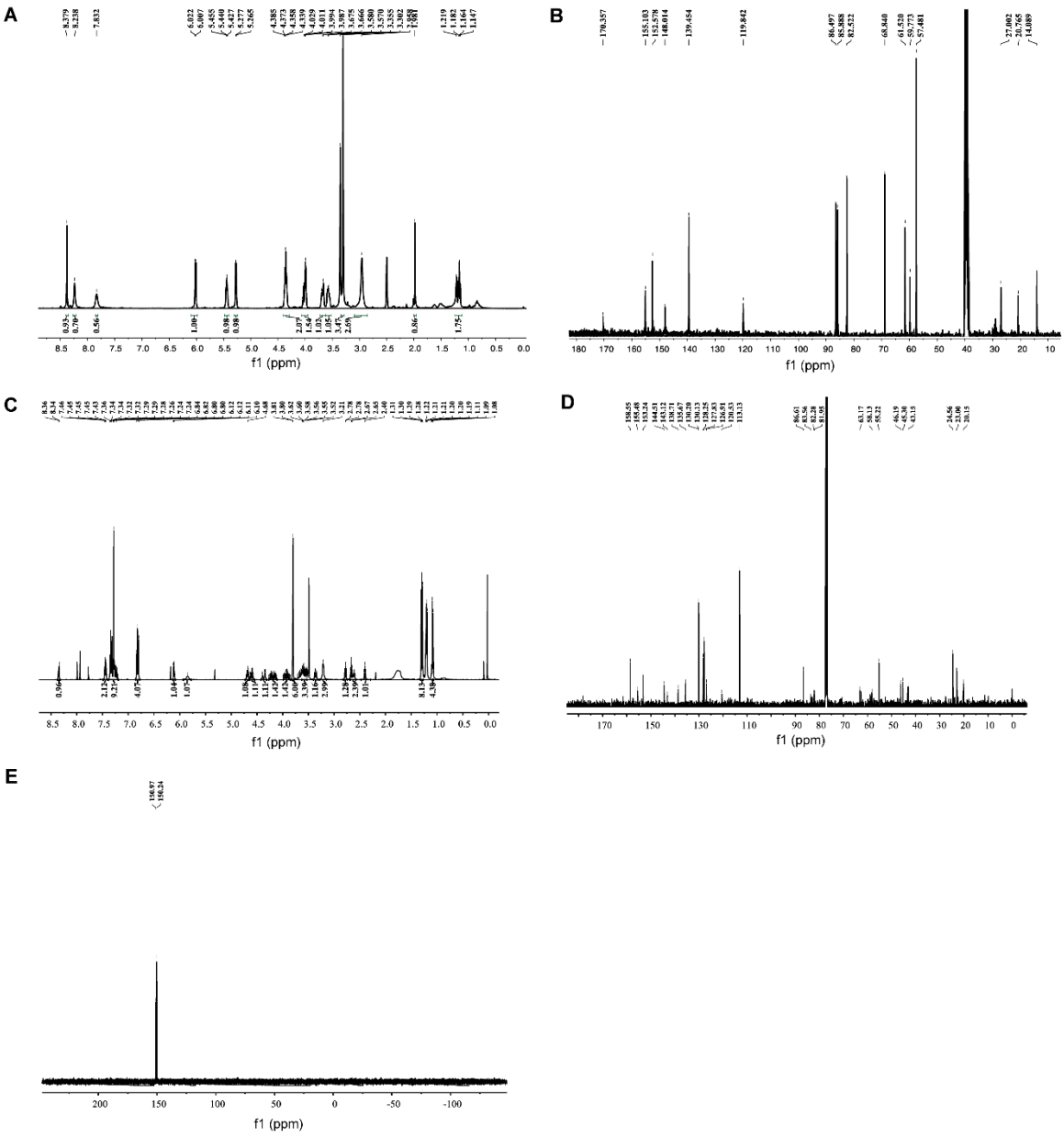

Fig. S14. NMR spectrums for synthesized m^6A_m standard nucleoside and phosphoramidite. (A)^{1}H-NMR and (B) ^{13}C-NMR for m^6A_m nucleoside. (C) ^{1}H-NMR, (D) ^{13}C-NMR, and (E) ^{33}P-NMR for m^6A_m phosphoramidite.

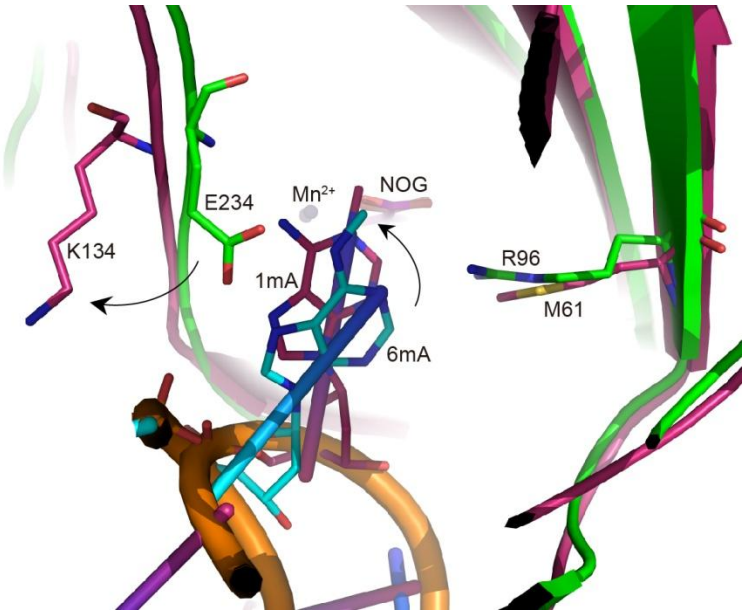

Fig. S15. Superposition of the FTO-6mA structure with the reported AlkB-1mA structure. The reported AlkB-1mA structure is colored in warm pink. The corresponding residues of FTO E234 and R96 in the AlkB-1mA structure are shown in sticks and labeled as K134 and M61 respectively. The black arrows indicate the rotation direction of 1mA base and K134 sidechain compared with 6mA base and E234 in the FTO-6mA structure.

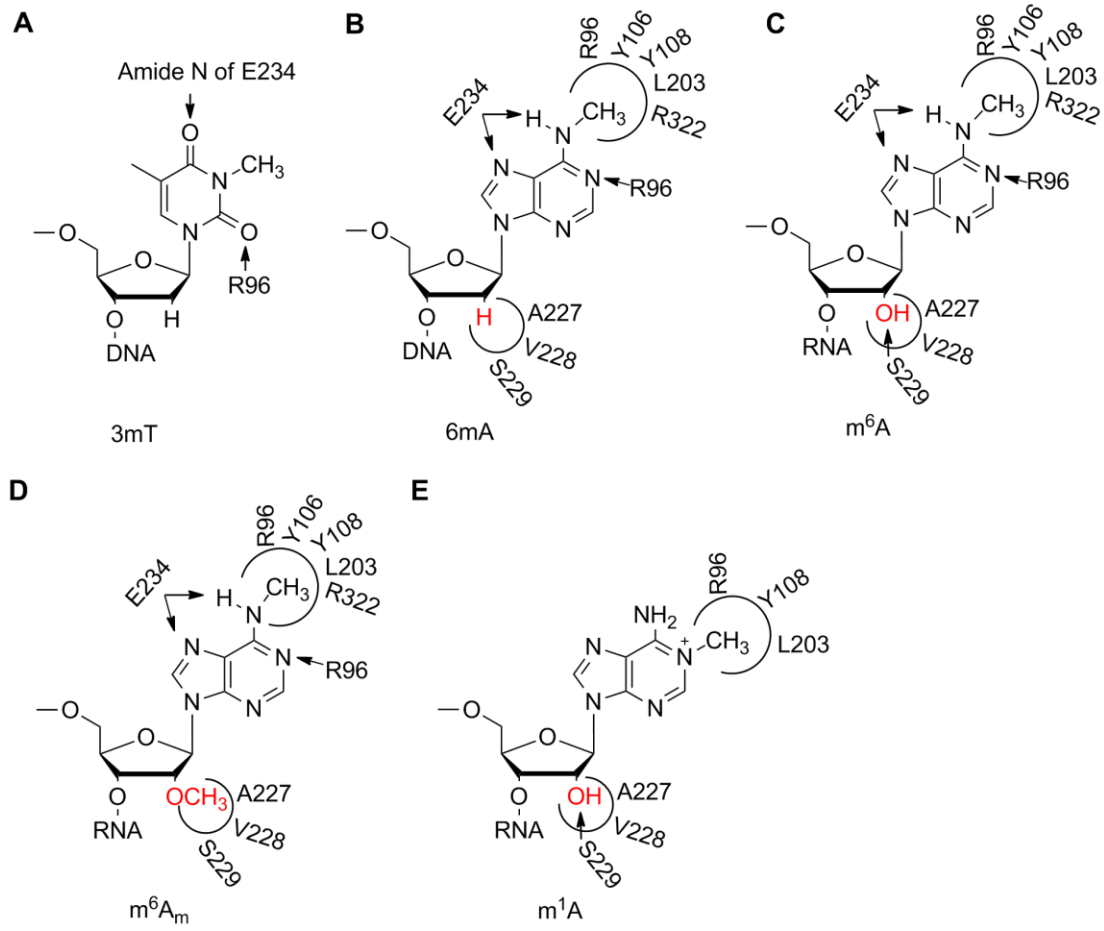

Fig. S16. Summary diagrams of the distinct recognition of FTO towards 3mT, 6mA, m^6A, m^6A_m and m^1A in the catalytic pocket. Protein residues forming direct hydrogen bonding interactions or a hydrophobic cavity are indicated. The group on the 2' position of the sugar ring of 6mA, m^6A, m^6A_m and m^1A are labeled in red color. Arrows indicate the H-bonds interaction. Half circle indicates a cavity.

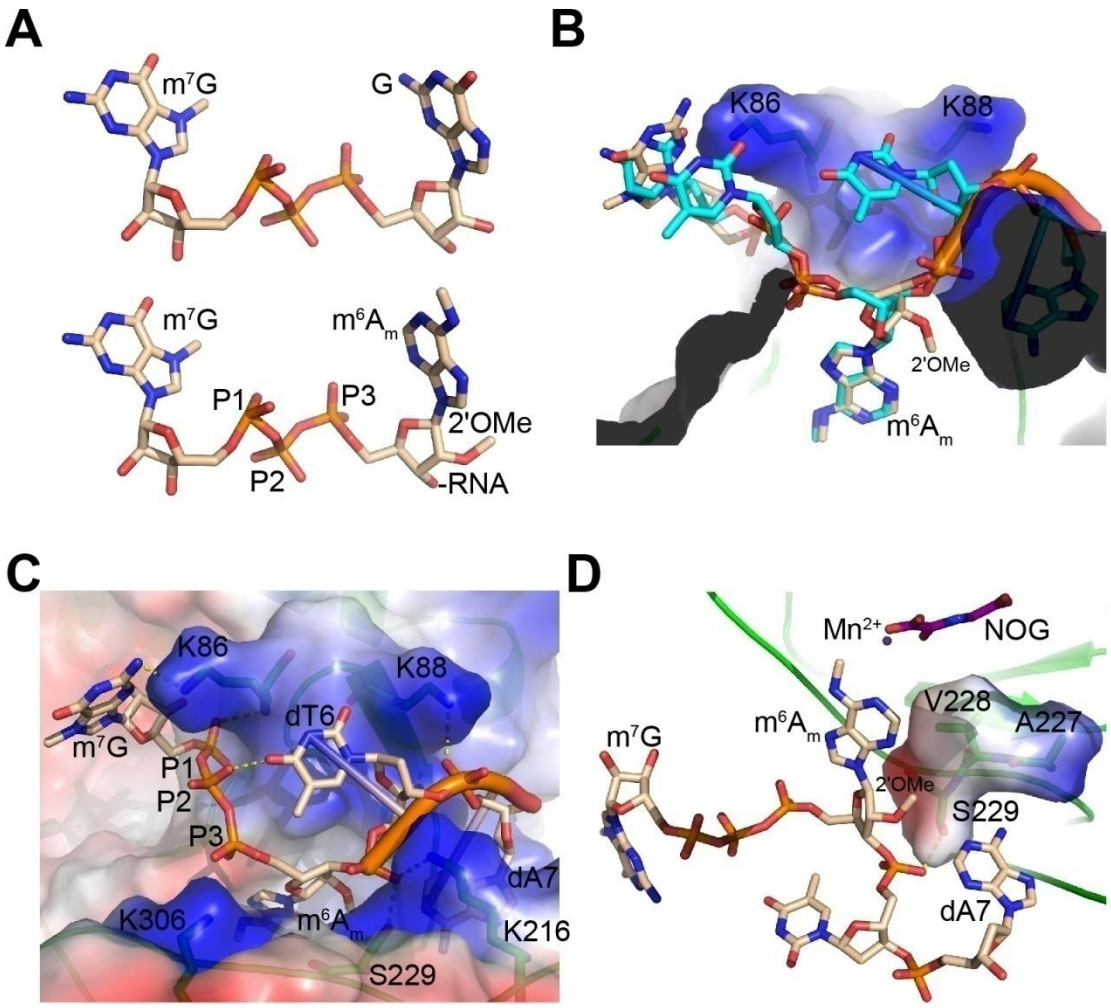

Fig. S17. Superposition of $m^7Gpppm^6A_m$ into the FTO-6mA structure. **(A)** The published cap structure of m^7GpppG and modeled structure of $m^7Gpppm^6A_m$. **(B)** Superposition of the cap structure $m^7Gpppm^6A_m$ into the FTO-6mA structure. **(C)** The interactions between the 2'OMe with FTO. The electrostatic surface of the small cave of FTO for 2'OMe group of m^6A_m accommodation is shown. **(D)** The electrostatic surface of the large space next to Pincer 2 for potential accommodation the m^7G cap.

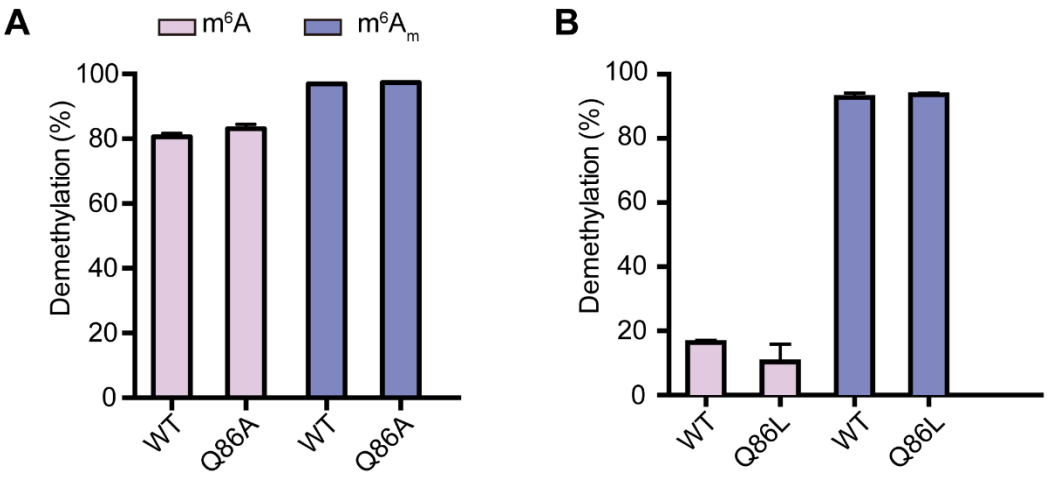

Fig. S18. Enzymatic activity comparison of wild-type (WT) and Q86 mutation of FTO in catalyzing m^6A and m^6A_m in isolated HeLa mRNA. 400 ng purified mRNA from HeLa cells *was treated* with 1 μM of WT or Q86A of FTO (A) 0.1 μM of WT or Q86L of FTO (B) and under standard demethylation conditions in 50 μl of reaction mixture for 1 h at 37 °C.

Substrate	Demethylation (%)
—AGm^{6}ACA—	87.1 ± 0.97
—AGm^{6}ACC—	86.7 ± 1.38
—GAm^{6}ACC—	84.0 ± 1.46
—AAm^{6}ACA—	81.7 ± 1.02
—GGm^{6}ACA—	78.1 ± 2.33
—GAm^{6}ACU—	77.6 ± 0.99
—AAm^{6}ACC—	74.4 ± 0.87
—GGm^{6}ACU—	73.8 ± 2.31
—UAm^{6}ACA—	72.3 ± 0.55
—AAm^{6}ACU—	70.6 ± 0.87
—GAm^{6}ACA—	66.4 ± 2.67
—AGm^{6}ACU—	54.5 ± 1.28
—GGm^{6}ACC—	43.8 ± 3.62

Fig. S19. The RNA sequence affects the catalytic activity of FTO. Oligo4 with different m^{6}A consensus sequence (10 μM) was incubated with 2 μM of FTO in 50 μl of reaction mixture for 10 min at 37 ℃. Data showed the mean ± s.d. (n=6, three biological replicates × two technical replicates).

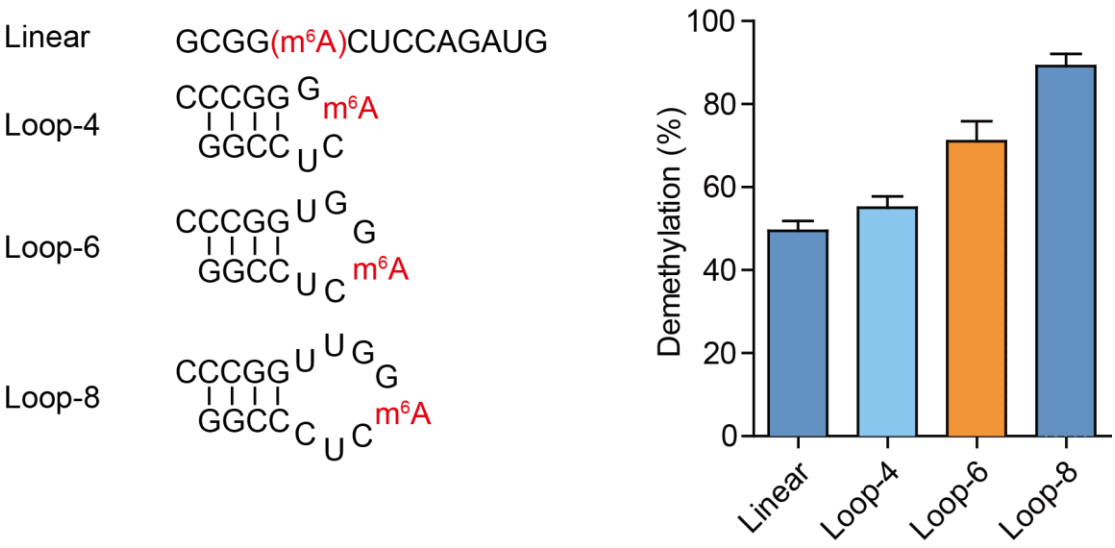

Fig. S20. The RNA tertiary structure affects the catalytic activity of FTO. FTO exhibits 2-fold higher demethylation activity for m^6A in a large stem loop than in a linear ssRNA. 10 μM of m^6A-modified Oligo was incubated with 1 μM of FTO in 50 μl of reaction mixture for 15 min at 37 ℃. Data showed the mean ± s.e.m. (n=6, three biological replicates × two technical replicates).

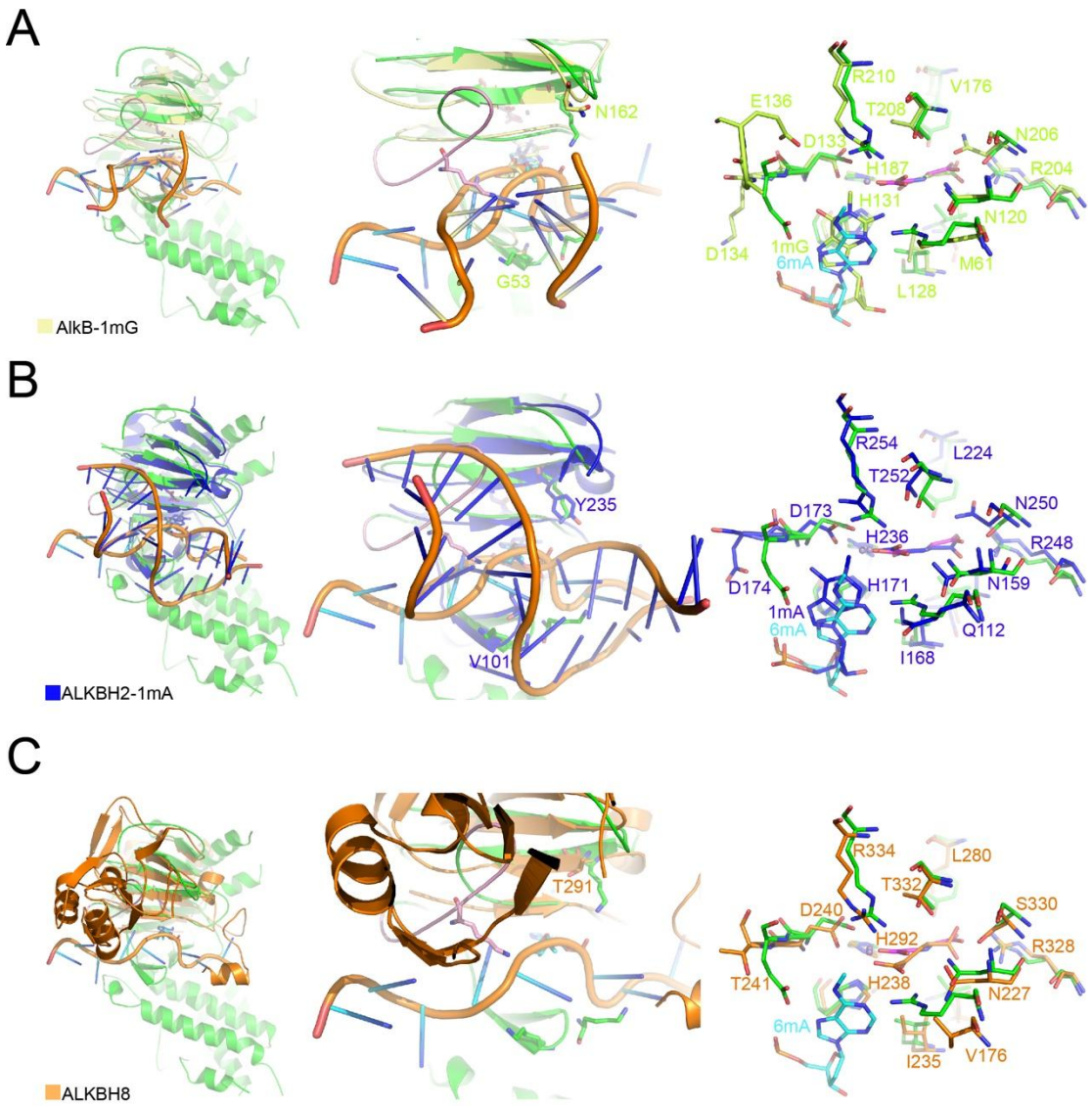

Fig. S21. Superposition of FTO-6mA structure with AlkB-1mG (PDB code: 3KHC) **(A),** ALKBH2-1mA (PDB code: 3BUC) **(B)**, and ALKBH8 (PDB code: 3THT) **(C)** structures**.** These structures are shown in green, paleyellow, blue, and orange respectively.

Supplementary Tables

Table S1. Data collection and refinement statistics

	FTO-ssDNA
Data collection	
Space group	*$I2_12_12_1$*
Cell dimensions	
a, *b*, *c*(Å)	*122.736, 160.033, 276.756*
α, β, γ (°)	*90.00, 90.00, 90.00*
Wavelength (Å)	*0.9785*
Resolution (Å)*	*50.0-3.3(3.42-3.3)*
R_{merge} (%)	*31.5(218)*
$I/\sigma I$	*7.9(1.04)*
Completeness (%)	*99.9(100)*
Redundancy	*7.0(7.1)*
Refinement	
Resolution (Å)	*37-3.3*
No.reflections	*1214474*
R_{work}/R_{free}	*0.271/0.291*
No.atoms	
Protein	*13034*
Nucleic acid	*732*
Water	*18*
Ligand/ion	*44*
B-factors	
Protein	*32.245*
Nucleic acid	*23.213*
Water	*22.787*
Ligand/ion	*18.617*
R.m.s deviations	
Bond lengths (Å)	*0.021*
Bond angles (°)	*2.1*

*Highest-resolution shell is shown in parentheses.

Table S2. Oligonucleotides used in this study

Name	Sequence (5'-3')	Purpose
hFTO_R96A_F	CTGCTGACCCCGGTTTCTGCTATTCTGATCGGTAATCC	Construction of the FTO mutants
hFTO_R96A_R	GGATTACCGATCAGAATAGCAGAAACCGGGGTCAGCAG	
hFTO_Y106F_F	GTAATCCTGGTTGCACCTTTAAATATCTGAACACCCG	
hFTO_Y106F_R	CGGGTGTTCAGATATTTAAAGGTGCAACCAGGATTAC	
hFTO_E234A_F	CTGGCACCACGACGCGAACCTGGTCGATC	
hFTO_E234A_R	GATCGACCAGGTTCGCGTCGTGGTGCCAG	
hFTO_Q86K_F	GTTTCGCGACCTGGTTCGTATTAAGGGCAAAGATC	
hFTO_Q86K_R	GATCTTTGCCCTTAATACGAACCAGGTCGCGAAAC	
hFTO_Q306K_F	CTGAACGCAACCCACAAGCACTGCGTTCTGG	
hFTO_Q306K_R	CCAGAACGCAGTGCTTGTGGGTTGCGTTCAG	
hFTO_S229A_F	TGGTGCCAGGCGACGGCCATTTTACCCATACCGAAG	
hFTO_S229A_R	AATGGCCGTCGCCTGGCACCACGACGAGAACCTGGT	
hFTO_E234P_F	CACCACGACCCCAACCTGGTCGATCGTTCTGCCGTG	
hFTO_E234P_R	GACCAGGTTGGGGTCGTGGTGCCAGGAGACGGCCAT	
hFTO_Q86A_F	GGTTCGTATTGCGGGCAAAGATCTG	
hFTO_Q86A_R	CAGATCTTTGCCCGCAATACGAACC	
hFTO_Q86L_F	CGACCTGGTTCGTATTCTGGGCAAAGATCTGCTG	
hFTO_Q86L_R	CAGCAGATCTTTGCCCAGAATACGAACCAGGTCG	
FAM-6mA-ssDNA	ATTGTCA6mACAGCAGA-FAM	Fluorescence anisotropy assay
6mA-ssDNA	ATCT6mATATCG	Crystallization
Oligo1	ATCT3mTTATCG	Demethylation activity assay *in vitro*
Oligo2	AUUGUCAm^{6}ACAGCAGC	
Oligo3	AUUGUCA(m^{6}A or m^{6}A$_m$)CAGCAGA	
Oligo4	AUUGUNNm^{6}ACNGCAGC (NNm^{6}ACN represents m^{6}A consensus sequence.)	
Linear ssRNA	GCGGm^{6}ACUCCAGAUG	
Loop-4	CCCGGGm^{6}ACUCCGG	
Loop-6	CCCGGUGGm^{6}ACUCCGG	
Loop-8	CCCGGUUGGm^{6}ACUCCCGG	

References

1. Strong M,Sawaya MR, Wang S, Phillips M, Cascio D, Eisenberg D (2006) Toward the structural genomics of complexes: crystal structure of a PE/PPE protein complex from Mycobacterium tuberculosis. *Proc Natl Acad Sci U S A*103: 8060-8065.
2. Han ZF, *et al.* (2010) Crystal structure of the FTO protein reveals basis for its substrate specificity. *Nature* 464: 1205-1209.
3. Emsley P, Cowtan K (2004) Coot: model-building tools for molecular graphics. *Acta Crystallogr D Biol Crystallogr*60: 2126-2132.
4. Schrodinger LLC(2017) The PyMOL molecular graphics system, Version 1.8.